Electronic Supplementary Information

Ultrathin MnO_2 nanoflakes grown on N-doped hollow carbon spheres for high-performance aqueous zinc ion batteries

Linlin Chen,[ab] Zhanhong Yang,[*a] Fan Cui,[ab] Jinlei Meng,[ab] Yinan Jiang,[ab] Jun Long[ab] and Xiao Zeng[ab]

a Hunan Province Key Laboratory of Chemical Power Source, College of Chemistry and Chemical Engineering, Central South University, Changsha, 410083, China

b Innovation Base of Energy and Chemical Materials for Graduate Students Training, Central South University, Changsha, 410083, China

** Corresponding author. E-mail address: zhyangcsu611@163.com (Z. Yang).*

Preparation of the Xanthan gum electrolyte

Xanthan gum electrolyte was prepared by a similar method mentioned in the previous research.[1] Typically, 10 g of xanthan gum powder (Aladdin, UPS class) was mixed with 50 mL aqueous solution consisted of 3 M $ZnSO_4$ and 0.15 M $MnSO_4$ at room temperature. After continuous mechanical agitation, a homogeneous gel electrolyte with good flexibility was obtained, which was utilized for the assembly of the flexible battery.

Fabrication of flexible Zn-MnO_2 battery

The flexible Zn-MnO_2 battery was assembled by separating the MnO_2-NHCSs cathode and Zn anode with PP nonwoven separator and xanthan gum electrolyte. After that, the battery was sealed by hot-pressing two pieces of polyethylene oxide films. The MnO_2-NHCSs cathode was prepared by coating a slurry consisted of 70 wt.% active material, 20 wt.% conductive agent (Super P) and 10 wt.% PTFE binder onto 0.1 mm stainless steel foil. The active area of the cathode was about 1.5×8 cm^2, and the total active material mass loading was about 20 mg (~1.67 mg cm^{-2}). A zinc foil (0.1 mm thickness) that was cut into 1.5 cm wide and 8 cm length was used as the anode.

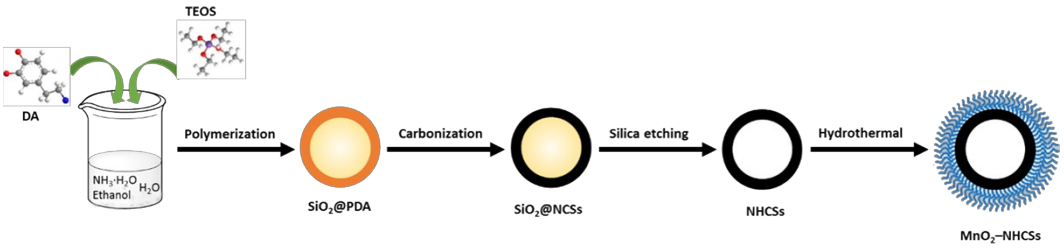

Fig. S1 Schematic illustration of the preparation of MnO_2-NHCSs.

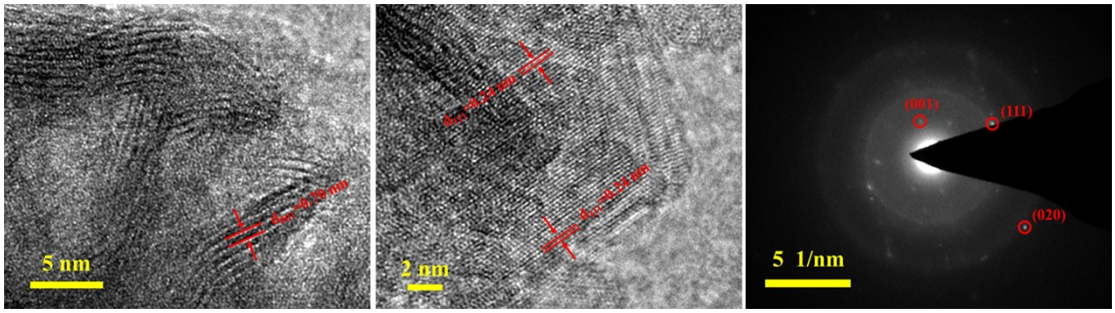

Fig. S2 (a,b) HRTEM images and (c) SAED pattern of the MnO_2-NHCSs sample.

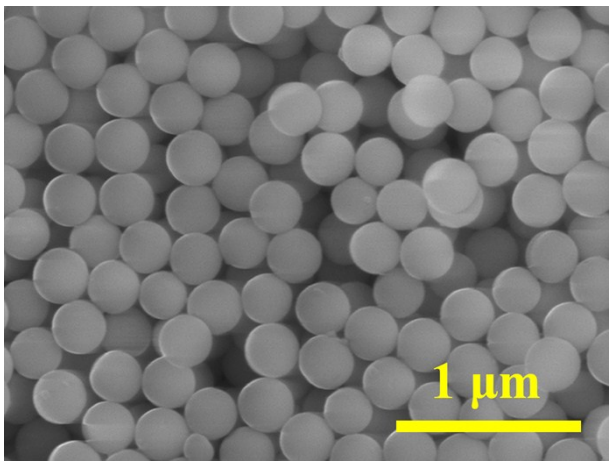

Fig. S3 SEM image of prepared SiO_2 spheres.

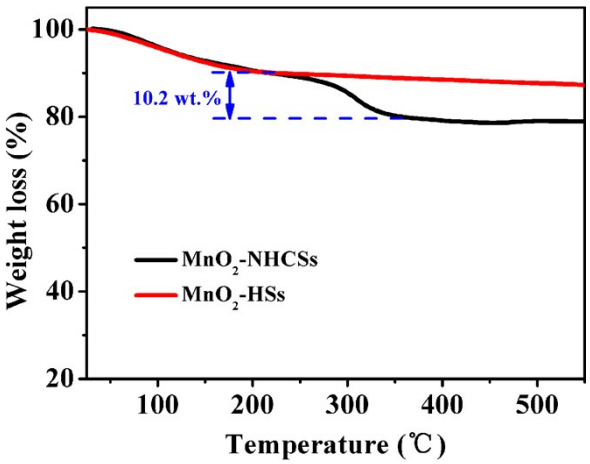

Fig. S4 TGA curves of MnO_2-NHCSs and MnO_2-HSs.

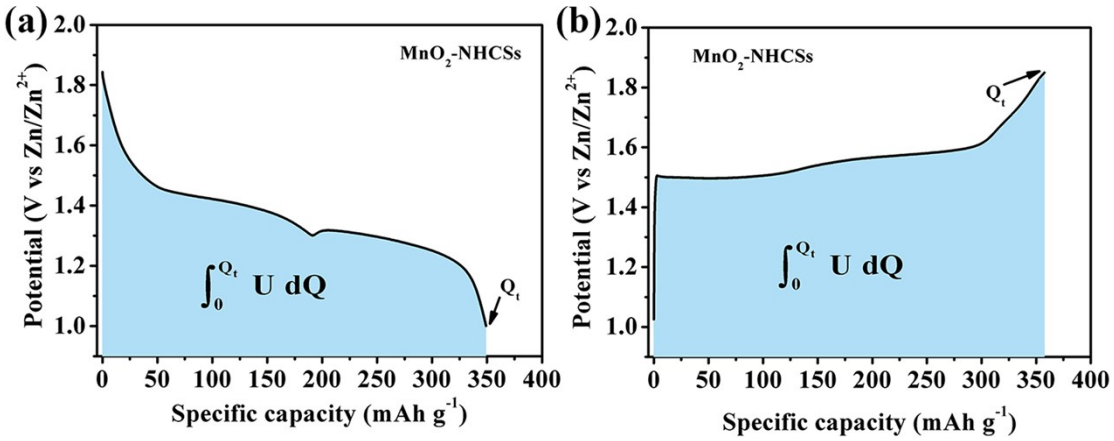

Fig. S5 The average voltage calculation based on the (a) discharge and (b) charge profiles of MnO_2-NHCSs in the 5th cycle at 0.1 A g^{-1}.

The average discharge/charge voltage ($\overline{U}$) can be estimated by the following formula:

$$\overline{U} = \frac{1}{Q_t}\int_0^{Q_t} U\, dQ \qquad (1)$$

Where U is the voltage, Q is specific capacity, and Q_t is the total capacity.

According to the constant current discharge and charge curves shown in Fig. S5, the average discharge and charge voltage were calculated to be 1.362 and 1.569 V, respectively.

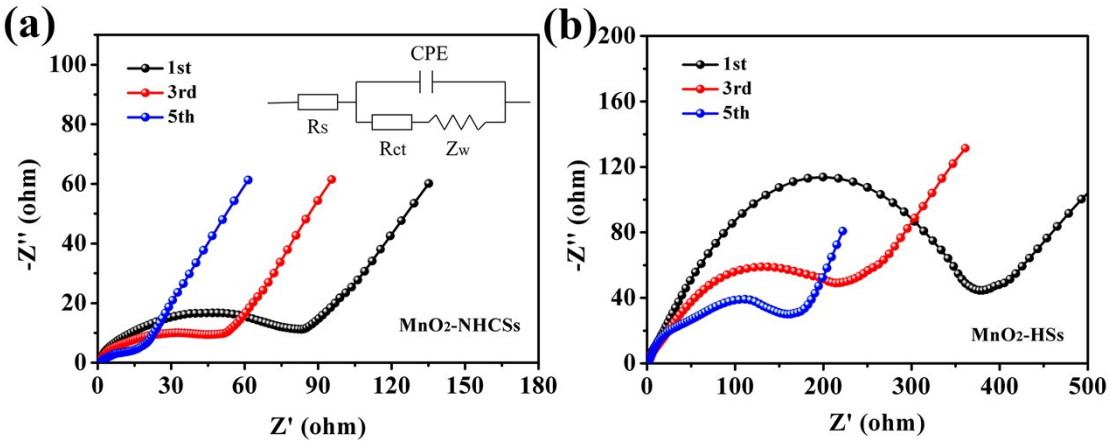

Fig. S6 Nyquist spectra of (a) MnO_2-NHCSs and (b) MnO_2-HSs, the cycled samples were controlled at the same charge state of 1.85 V. Inset of (a) shows the equivalent circuit diagram, Rs: solution resistance, Rct: charge transfer resistance, CPE: constant-phase element, Zw: Warburg impedance.

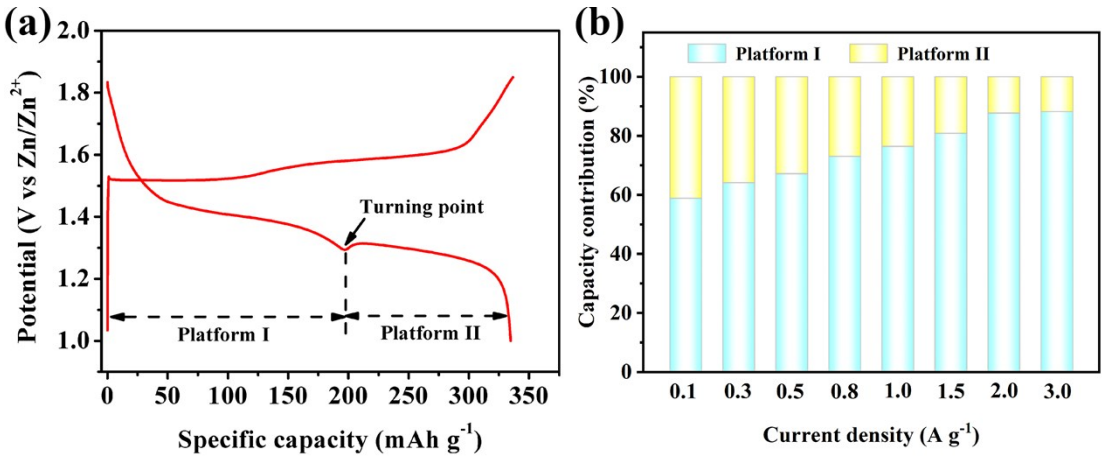

Fig. S7 (a) Demarcation of the discharge platform by turning point, (b) the capacity contribution of platform I and II to the total capacity.

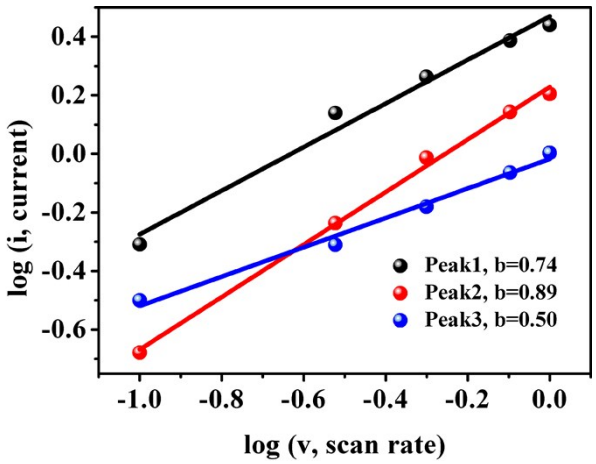

Fig. S8 Logarithmic diagrams of current (i) and scan rate (v) at specific peak currents.

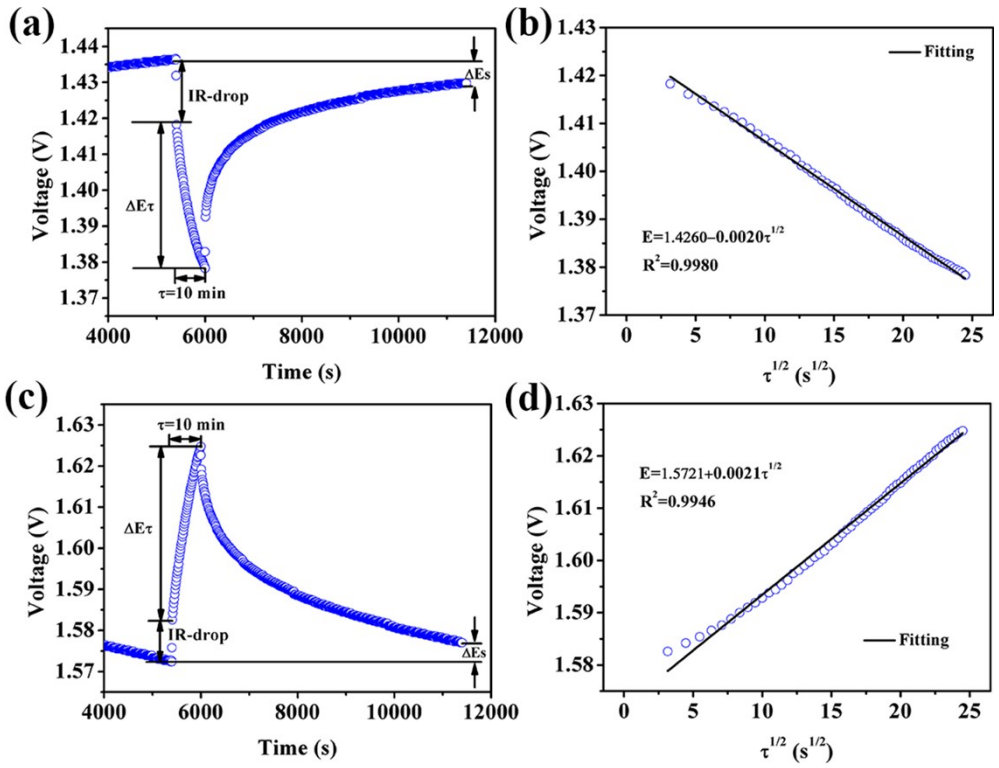

Fig. S9 Single GITT profiles and linear behaviour of the transient voltage changes E vs. $\tau^{1/2}$ for the MnO_2-NHCSs electrode during the discharge (a,b) and charge (c,d) process.

In order to gain the Zn^{2+} diffusion coefficient of the MnO_2-NHCSs electrode, GITT tests were carried out during the 6th cycle. In GITT measurement, the cell was charged or discharged at 0.05 A g^{-1} for 10 min, followed by an open circuit stand for 90 min, allowing the cell voltage to relax to its steady-state value. The procedure was repeated until the battery reached to the cut off voltage (1.85 or 1.0 V). The diffusion coefficient of Zn^{2+} (D_{Zn}, cm^2 s^{-1}) are calculated based on the following equation:[2,3]

$$D_{Zn} = \frac{4}{\pi\tau}\left(\frac{m_B v_m}{M_B S}\right)^2\left(\frac{\Delta E_s}{\Delta E_\tau}\right)^2 \quad (1)$$

Where, τ (s) is the pulse duration of constant current, m_B (g), M_B (g mol^{-1}), and v_m (cm^3 mol^{-1}) correspond to the quality, molar mass, and molar volume of the active material, respectively, S (cm^2) is the contacting area of electrode with electrolyte (taken as the geometric area of electrode for better comparison with literatures), ΔE_S is the voltage change of the termination voltage of two adjacent relaxation steps, ΔE_τ is the potential change during the constant current pulse after eliminating the IR-drop.

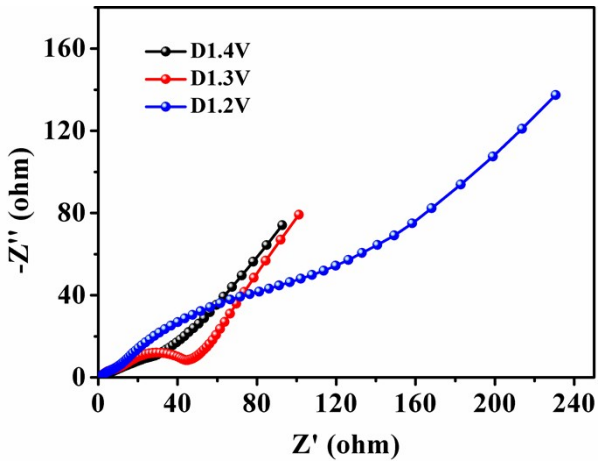

Fig. S10 Nyquist spectra of MnO_2-NHCSs taken at different discharge states.

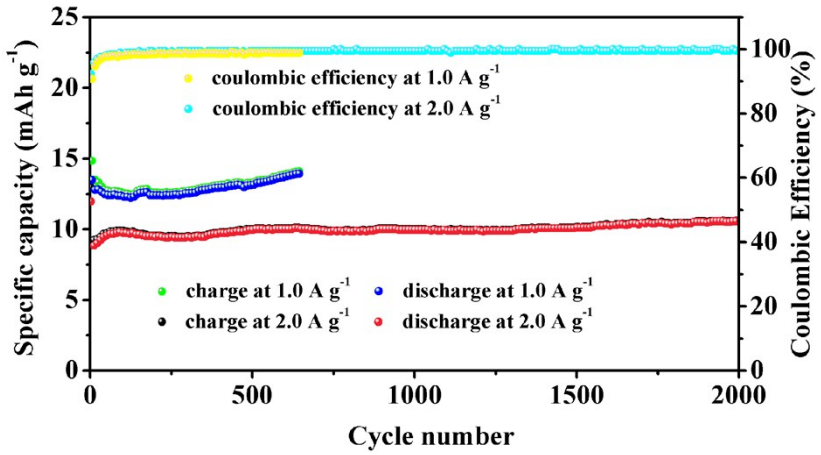

Fig. S11 The cyclic performance of NHCSs at 1.0 A g^{-1} and 2.0 A g^{-1}.

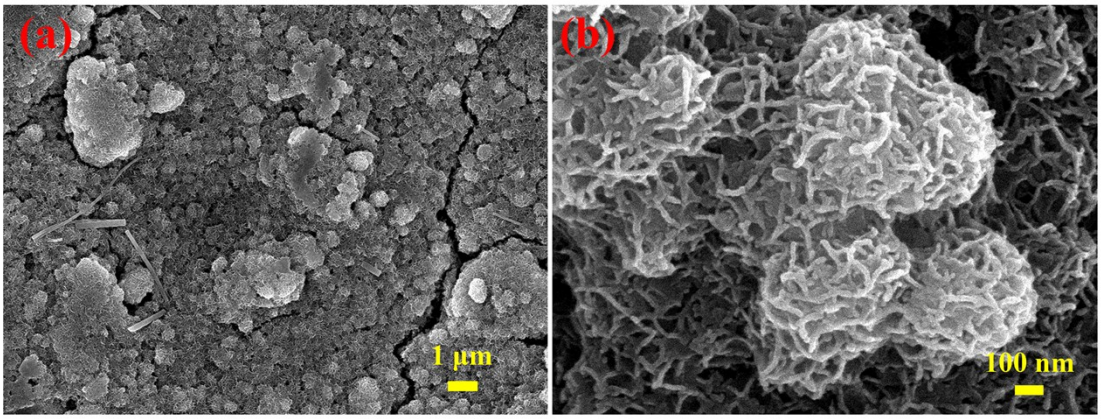

Fig. S12 SEM images of the MnO_2-NHCSs electrode after 100 cycles at 1.0 A g^{-1}.

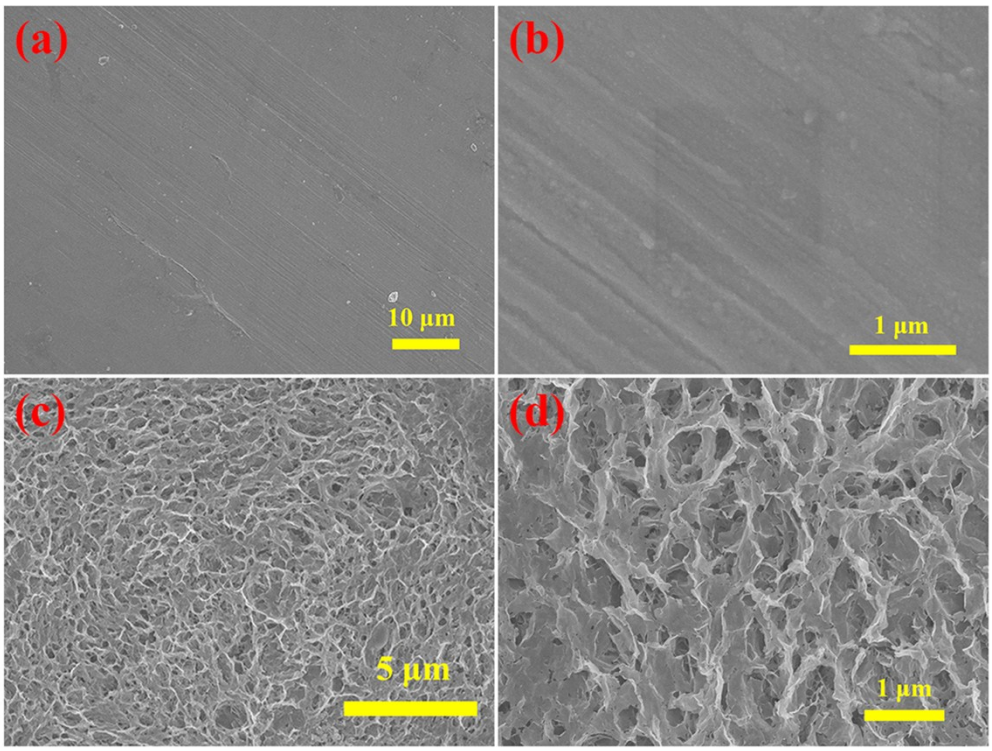

Fig. S13 SEM images of (a,b) pristine Zn plate and (c,d) Zn anode after charging and discharging at 1.0 A g^{-1} for 100 cycles.

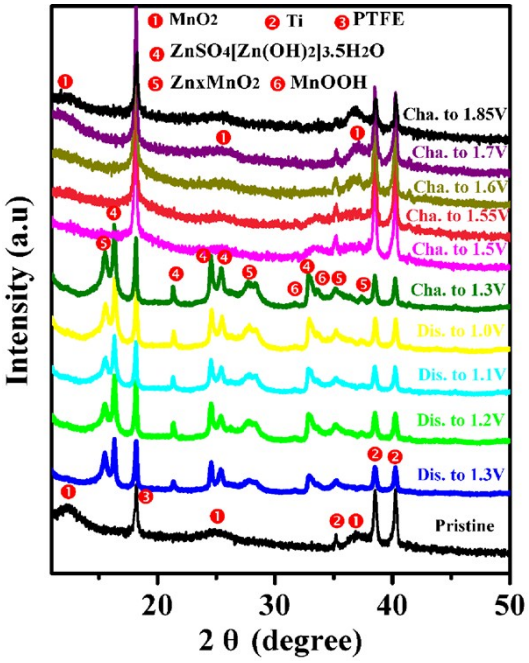

Fig. S14 Ex-situ XRD patterns of the MnO_2-NHCSs electrode at different charge/discharge states.

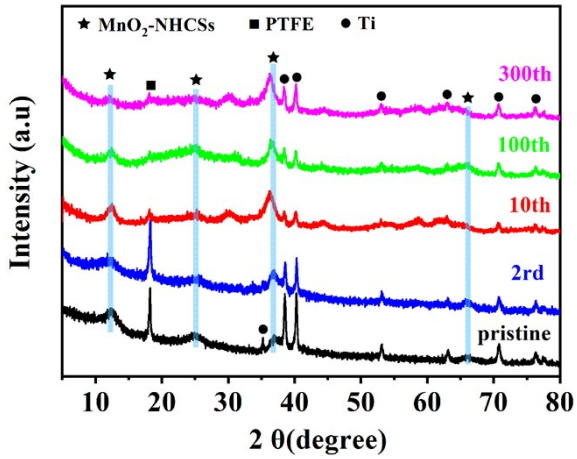

Fig. S15 Ex-situ XRD patterns of the MnO_2-NHCSs electrode after different cycles.

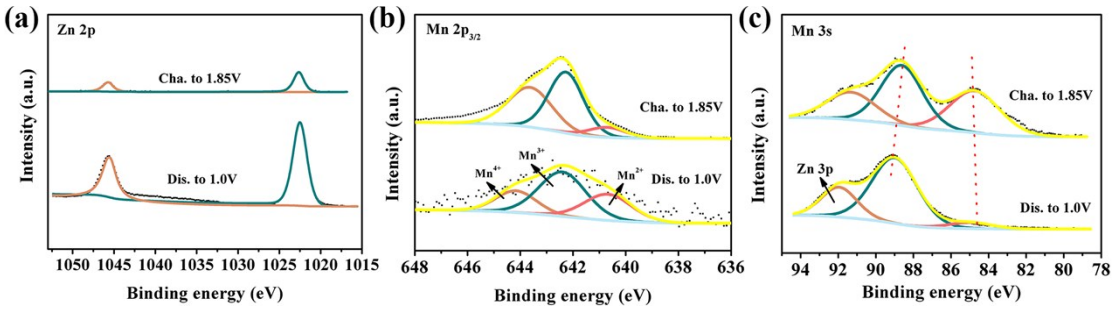

Fig. S16 Ex-situ XPS spectra of the MnO_2-NHCSs electrode at fully discharged/charged states, (a) Zn 2p, (b) Mn 2p, (c) Mn 3s.

Table S1. Specific surface area and pore size parameters of MnO_2-NHCSs and MnO_2-HSs.

Sample	Surface area (m^2 g^{-1})	Pore volume (cm^3 g^{-1})	Average pore size (nm)
MnO_2-NHCSs	213.12	0.61	13.52
MnO_2-HSs	141.24	0.83	25.98

Table S2. Electrochemical performance comparisons of the MnO_2-NHCSs electrode with other previously reported manganese-based oxide cathodes.

Electrode	Electrolyte	Rate capability	Cycling stability	Ref.
a-MnO_2 nanorod	1 M $ZnSO_4$	233/0.083, 31/1.666	147/63%/0.083/50	4
Todorokite-type MnO_2	1 M $ZnSO_4$	108/0.05	-/100%/0.05/50	5
δ-MnO_2 nanoflake	1 M $ZnSO_4$	252/0.083, 30/1.333	112/-/0.083/100	6
Cation-Deficient $ZnMn_2O_4$	3 M $Zn(CF_3SO_3)_2$	150/0.05, 72/2.0	80/94%/0.5/500	7
a-MnO_2 nanorod	1 M $ZnSO_4$	323/0.016, 47/1.666	104/-/0.083/75	8
V-doped MnO_2	1 M $ZnSO_4$	266/0.066	131/49.2%/0.066/100	9
α-MnO_2@C	1 M $ZnSO_4$	272/0.066	189/69.5%/0.066/50	10
ZnHCF@MnO_2	0.5 M $ZnSO_4$	118/0.1, 75.2/1.0	~70/77%/0.5/1000	11
$ZnMn_2O_4$	1 M $ZnSO_4$+0.05 M $MnSO_4$	70.2/3.2	106.5/100%/0.1/300	12

MnO_2@CFP	2 M $ZnSO_4$+0.2 M $MnSO_4$	290/0.09	50−70/100%/1.885/10000	13
Mn_2O_3	2 M $ZnSO_4$+0.1 M $MnSO_4$	137/0.2, 38/2.0	82.2/-/2.0/1000	14
SSWM@Mn_3O_4	2 M $ZnSO_4$+0.1 M $MnSO_4$	296/0.1, 125/0.5	296/98%/0.1/50	15
MnO_2-NHCSs	3 M $ZnSO_4$+ 0.15 M $MnSO_4$	348/0.1, 127/3.0	349/100%/0.1/80 100/78.7%/2.0/2000	**This work**

Explanation of the above data implications: take the first a-MnO_2 nanorod as an example, i) Rate capability, 233/0.083, 31/1.666 present that 233 mAh g^{-1} at 0.083 A g^{-1}, and 31 mAh g^{-1} at a high rate of 1.666 A g^{-1}; ii) Cycling stability, 147/63%/0.083/50 present that 147 mAh g^{-1} (capacity retention of 63%) was retained at 0.083 A g^{-1} after 50 cycles.

References

1 S. L. Zhang, N. S. Yu, S. Zeng, S. S. Zhou, M. H. Chen, J. T. Di and Q. W. Li, *J. Mater. Chem. A*, 2018, **6**, 12237−12243.

2 H. G. Qin, L. L. Chen, L. M. Wang, X. Chen and Z. H. Yang, *Electrochim. Acta*, 2019, **306**, 307−316.

3 L. L. Chen, Z. H. Yang and Y. G. Huang, *Nanoscale*, 2019, **11**, 13032−13039.

4 M. H. Alfaruqi, J. Gim, S. Kim, J. J. Song, J. Jo, S. Kim, V. Mathew and J. Kim, *J. Power Sources*, 2015, **288**, 320−327.

5 J. Lee, J. B. Ju, W. I. Cho, B. W. Cho and S. H. Oh, *Electrochim. Acta*, 2013, **112**, 138−143.

6 M. H. Alfaruqi, J. Gim, S. J. Kim, J. J. Song, D. T. Pham, J. Jo, Z. L. Xiu, V. Mathew and J. Kim, *Electrochem. Commun*., 2015, **60**, 121−125.

7 N. Zhang, F. Y. Cheng, Y. C. Liu, Q. Zhao, K. X. Lei, C. C. Chen, X. S. Liu and J. Chen, *J. Am. Chem. Soc*., 2016, **138**, 12894−12901.

8 M. H. Alfaruqi, S. Islam, J. Gim, J. J. Song, S. J. Kim, D. T. Pham, J. Jo, Z. L. Xiu, V. Mathew and J. Kim, *Chem. Phys. Lett*., 2016, **650**, 64−68.

9 M. H. Alfaruqi, S. Islam, V. Mathew, J. J. Song, S. J. Kim, D. P. Tung, J. Jo, S. Kim, J. P. Baboo, Z. L. Xiu and J. Kim, *Appl. Surf. Sci*., 2017, **404**, 435−442.

10 S. Islam, M. H. Alfaruqi, J. Song, S. Kim, D. T. Pham, J. Jo, S. Kim, V. Mathew, J. P. Baboo, Z. L. Xiu and J. Kim, *J Energy Chem*., 2017, **26**, 815−819.

11 K. Lu, B. Song, Y. X. Zhang, H. Y. Ma and J. T. Zhang, *J. Mater. Chem. A*, 2017, **5**, 23628−23633.

12 X. W. Wu, Y. H. Xiang, Q. J. Peng, X. S. Wu, Y. H. Li, F. Tang, R. C. Song, Z. X. Liu, Z. Q. He and X. M. Wu, *J. Mater. Chem. A*, 2017, **5**, 17990−17997.

13 W. Sun, F. Wang, S. Hou, C. Y. Yang, X. L. Fan, Z. H. Ma, T. Gao, F. D. Han, R. Z. Hu, M. Zhu and C. S. Wang, *J. Am. Chem. Soc*., 2017, **139**, 9775−9778.

14 B. Z. Jiang, C. J. Xu, C. L. Wu, L. B. Dong, J. Li and F. Y. Kang, *Electrochim. Acta*, 2017, **229**, 422−428.

15 C. Y. Zhu, G. Z. Fang, J. Zhou, J. H. Guo, Z. Q. Wang, C. Wang, J. Y. Li, Y. Tang and S. Q. Liang, *J. Mater. Chem. A*, 2018, **6**, 9677−9683.